



**HAL**  
open science

# Anisotropy and Deformation Processes in Southern California From Rotational Observations

Le Tang, Heiner Igel, Jean-Paul Montagner

► **To cite this version:**

Le Tang, Heiner Igel, Jean-Paul Montagner. Anisotropy and Deformation Processes in Southern California From Rotational Observations. *Geophysical Research Letters*, 2023, 50, 10.1029/2023GL105970 . insu-04462227

**HAL Id: insu-04462227**

**<https://insu.hal.science/insu-04462227>**

Submitted on 19 Feb 2024

**HAL** is a multi-disciplinary open access archive for the deposit and dissemination of scientific research documents, whether they are published or not. The documents may come from teaching and research institutions in France or abroad, or from public or private research centers.

L'archive ouverte pluridisciplinaire **HAL**, est destinée au dépôt et à la diffusion de documents scientifiques de niveau recherche, publiés ou non, émanant des établissements d'enseignement et de recherche français ou étrangers, des laboratoires publics ou privés.



Distributed under a Creative Commons Attribution - NonCommercial - NoDerivatives 4.0 International License



# Geophysical Research Letters<sup>®</sup>



## RESEARCH LETTER

10.1029/2023GL105970

## Anisotropy and Deformation Processes in Southern California From Rotational Observations

Le Tang<sup>1</sup> , Heiner Igel<sup>1</sup>, and Jean-Paul Montagner<sup>2</sup> 

<sup>1</sup>Department of Earth and Environmental Sciences, Ludwig-Maximilians-Universität München, Munich 80333, Germany,

<sup>2</sup>Institut de Physique du Globe de Paris, Université de Paris, Paris, France

### Key Points:

- Local seismic anisotropy revealed for the first time from rotational amplitude observations
- Depth dependence of anisotropy in the local upper mantle of Southern California region is well resolved in lateral and vertical directions
- The asthenospheric fast axis matches absolute plate motions, providing new insights on geodynamic processes in Southern California

### Supporting Information:

Supporting Information may be found in the online version of this article.

### Correspondence to:

L. Tang,  
[Le.Tang@lmu.de](mailto:Le.Tang@lmu.de)

### Citation:

Tang, L., Igel, H., & Montagner, J.-P. (2023). Anisotropy and deformation processes in Southern California from rotational observations. *Geophysical Research Letters*, 50, e2023GL105970. <https://doi.org/10.1029/2023GL105970>

Received 16 AUG 2023

Accepted 20 NOV 2023

### Author Contributions:

**Conceptualization:** Le Tang, Heiner Igel, Jean-Paul Montagner

**Data curation:** Le Tang

**Formal analysis:** Le Tang

**Funding acquisition:** Heiner Igel, Jean-Paul Montagner

**Investigation:** Le Tang

**Methodology:** Le Tang

**Project Administration:** Heiner Igel, Jean-Paul Montagner

**Visualization:** Le Tang, Heiner Igel, Jean-Paul Montagner

**Writing – original draft:** Le Tang

**Writing – review & editing:** Le Tang, Heiner Igel, Jean-Paul Montagner

© 2023 The Authors.

This is an open access article under the terms of the [Creative Commons Attribution-NonCommercial License](https://creativecommons.org/licenses/by-nc/4.0/), which permits use, distribution and reproduction in any medium, provided the original work is properly cited and is not used for commercial purposes.

**Abstract** Seismic anisotropy in the upper mantle reveals geodynamic processes and the tectonic evolution of the Earth. The two most powerful methods, surface wave tomography, and shear-wave splitting observations, cannot investigate the deep local anisotropy with good vertical and lateral resolution, resulting in poor constraints on plate deformation processes of the complex plate boundary beneath the Southern California region. Here, we show that the amplitude ratio of translational displacement and rotation makes it possible to retrieve the local anisotropy in the upper mantle. Azimuthal anisotropy in the asthenosphere is well determined and resolved in lateral and vertical directions. The fast axis retrieved from amplitude observations indicates the local rapid changes in plate deformation and complex pattern of mantle flow, which is compatible with the distributions of horizontal mantle flow illuminated by geodetic measurements, providing new insights on geodynamic processes of the Southern California region.

**Plain Language Summary** Rotational motion is the angle of ground rotation observed during Earth's deformation, and the ratio of amplitude to translational motion is sensitive to local structure. In the past few decades, study on the mantle structure inside the Earth has mainly relied on the time difference of seismic waves to calculate azimuth-dependent velocity changes, namely azimuthal anisotropy. Due to the correlation between the direction of maximum velocity propagation and the direction of mantle flow and plate deformation, the study of mantle anisotropy can provide evidence for the evolution of the Earth. However, studying anisotropy based on seismic wave travel time is often affected by heterogeneity, especially in extremely complex structures such as Southern California. The splitting of shear waves can effectively constrain the anisotropy of the mantle in the lateral direction, but its depth resolution is poor. Additional rotational amplitude observations with local sensitivity and depth resolution can provide better constraints on the study of mantle anisotropy, providing new evidence for the direction of mantle flow and plate motion.

## 1. Introduction

Seismic anisotropy is a powerful diagnostic tool providing access to information on the orientation of small scale heterogeneities (e.g., cracked, porous media, crystals, bedding (Anderson et al., 1974; Crampin, 1978)) that—in many cases—are aligned according to the local stress or strain field. In turn, principal stress/strain directions can be associated with the direction of mantle flow (Ghosh & Holt, 2012; Montagner, 1994; Ribe, 1989; Tanimoto & Anderson, 1984). Thus, extracting anisotropic properties plays a significant role in understanding subsurface processes such as tectonic motions, reservoir behavior, or stress evolution.

On regional scales, there are two key methodologies to estimate anisotropic parameters. First, the phenomenon of shear-wave splitting (Crampin et al., 1980) of near-vertically propagating waves (e.g., SKS phase (Silver & Chan, 1988; Vinnik et al., 1984)) can be used to estimate the polarization of the fast quasi-shear wave. It is assumed that this polarization is associated with the dominant horizontal stress/strain direction (Crampin & Lovell, 1991). This method has the advantage that a single three-component seismic station can provide the required information. The disadvantage is the lack of resolution with depth (Savage, 1999). Second, surface wave observations from many azimuths observed on a sufficiently scaled seismic array can be used to determine azimuthal anisotropy from Love or Rayleigh waves (Forsyth, 1975). This approach—while having some depth resolution through the frequency-dependence of surface wave phase velocities (Montagner & Nataf, 1986)—has a poor lateral resolution. Regional full-waveform inversion approaches (Zhu & Tromp, 2013) intrinsically also provide access to anisotropic parameters by exploiting surface wave phase information across a broad frequency range, but still with a limited lateral resolution.

The local deformation can be divided into a symmetric part (the strain tensor) and an antisymmetric part (three components of rotation). Both are sensitive to seismic anisotropy (Tang et al., 2023). In the past few years—through the emergence of multi-component rotational ground motion instruments such as ring lasers (Igel et al., 2005, 2021; Schreiber et al., 2014) or fiber-optic gyros (Schreiber et al., 2009)—techniques were developed to exploit the resulting 6-degrees-of-freedom observations (6 dof, three components of rotations and three components of translations) opening a new range of opportunities in particular for single-station observations. Most notably, 6 dof observations provide direct access to local surface wave phase velocities and propagation directions through the analysis of amplitude ratios (Igel et al., 2007), which is capable of extracting the dispersion of different modes of surface waves (Tang & Fang, 2023). By applying adjoint techniques (Fichtner & Igel, 2009) to such joint observations, it could be shown that 6 dof point measurements are sensitive to near-receiver structure, eliminating the path effects of wave propagation.

Here, we apply for the first time the emerging 6 dof technology to the estimation of local anisotropic parameters in the upper mantle from surface wave observations. As currently no (portable) rotation sensing system exists that allows the analysis of multi-azimuth observations, we resort to so-called array-derived rotation (ADR) (Spudich & Fletcher, 2008; Spudich et al., 1995) that makes use of wavefield gradient estimations from surface seismic arrays in appropriate frequency bands.

Southern California—characterized by a complex tectonic and geodynamic environment—is the best location to apply our new approach. The dense broadband seismic networks in California that have operated for decades allow us to use station subsets as arrays and use ADR techniques to estimate rotations and subsequently apply single-station techniques to the resulting 6 dof data. We investigate how the frequency-dependent anisotropic parameters are consistent with other geophysical or geodetic observations and how it provides new information at depth on the layering and change of orientation of azimuthal anisotropy, as the 6 dof approach has a substantially higher lateral resolution for upper mantle anisotropy study than other techniques. Our study motivates the development of high-sensitivity rotation sensors to further extend the potential of 6 dof observations toward the inversion for anisotropy parameters from point measurements.

## 2. Methods

### 2.1. Azimuthal Anisotropy From Rotational Observations

Our recent theory paper (Tang et al., 2023) demonstrates that the amplitude ratio of acceleration to rotational velocity or strain velocity is equal to the analytical azimuth-dependent phase velocity of the corresponding surface wave (Smith & Dahlen, 1973). Since the fundamental Rayleigh wave is generally far away from Love wave modes, the coupled wavefield has small effects on the Rayleigh wave amplitude. In this paper, we only consider the fundamental mode of the quasi-Rayleigh wave. The dispersion equation of the dominant quasi-Rayleigh wave from the amplitude ratio can be expressed as (Tang et al., 2023):

$$\left| \frac{A_z(\omega, \psi)}{\Omega_r(\omega, \psi)} \right| = c_{R0}(\omega) + \frac{1}{2c_{R0}(\omega)} [R_1(\omega) + R_2(\omega) \cos(2\psi) + R_3(\omega) \sin(2\psi) + R_4(\omega) \cos(4\psi) + R_5(\omega) \sin(4\psi)] \quad (1)$$

where  $A_z(\omega, \psi)$  is the vertical acceleration and  $\Omega_r(\omega, \psi)$  is the transverse rotational velocity.  $\psi$  is the backazimuth of the wavenumber vector measured clockwise from the north direction.  $c_{R0}(\omega)$  is the phase velocity of the Rayleigh wave for the isotropic medium considered as a reference model.  $R_i(\omega)$  ( $i = 1, 2, 3, 4, 5$ ) are respectively depth integration functions that involve some elastic parameters and eigenfunctions, where we used a simple integration expression derived by Montagner and Nataf (1986), whose explicit expressions can be found in Equations 2, 4, and 5 of Montagner and Nataf (1986).

Equation 1 provides a new method for estimating phase velocities in anisotropic media which only depends on amplitude information. Its sensitivity kernel attains large absolute values only in the vicinity of the receiver but not in the vicinity of the source (Fichtner & Igel, 2009) which means that the phase velocity is only sensitive to the local structure. Its lateral resolution can be several times smaller than one wavelength (Tang & Fang, 2023).

## 2.2. Phase Velocity Smoothing and Variance

To investigate the azimuth-dependent variation in phase velocity, we set up a simple function to smooth the phase velocity points in each period, where the smoothed phase velocity and the standard deviation  $\sigma$  can be expressed as

$$\overline{c_R}(\omega, \psi) = \frac{\sum_{\psi_1=\psi'-\psi_0}^{\psi_1=\psi'+\psi_0} c_R(\omega, \psi_1)}{N}, \psi = \frac{\sum_{\psi_1=\psi'-\psi_0}^{\psi_1=\psi'+\psi_0} \psi_1}{N}, \psi' \in [0, 2\pi] \quad (2)$$

$$\sigma(\omega, \psi) = \sqrt{\frac{\sum_{\psi_1=\psi'-\psi_0}^{\psi_1=\psi'+\psi_0} [c_R(\omega, \psi_1) - \overline{c_R}(\omega, \psi)]^2}{N}} \quad (3)$$

where  $\psi_0$  is the selected azimuth window width and  $N$  represents the number of dispersion points from  $\psi' - \psi_0$  to  $\psi' + \psi_0$ . In the following data analysis, the azimuth window  $\psi_0$  is equal to  $60^\circ$  and  $\psi'$  is from  $0$  to  $360^\circ$  in one degree interval. The selection of the azimuth window is a trade-off when considering the large waveform error of ADR and the best fit between the data and the theoretical anisotropy curve.

## 3. Data

The earthquake data comes from the CI station network (see support information file for station names), and SCEDC (southern California Seismic Network) data center. Considering that broadband rotational seismometers have not been permanently deployed widely, we selected high-quality permanent broadband seismographs in Southern California region as an array for retrieving rotational motions by using the ADR approach (Spudich et al., 1995; Spudich & Fletcher, 2008). We select 110 teleseismic earthquakes with a magnitude larger than 7.0 (only a few events are between 6.5 and 7.0, see Figure S1 in Supporting Information S1) from the global earthquake catalog from November 2014 to November 2022.

Due to the uneven distribution of permanent stations in Southern California, it is necessary to choose a station array with high waveform quality and evenly spaced distribution at all azimuths as much as possible when using the ADR method. To have sufficient available stations, the minimum distance of the stations we selected is around 20 km (see Figure S2 in Supporting Information S1), as the spacing between these permanent stations in Southern California is mostly larger than 20 km. The minimum aperture limits the high-frequency threshold, while the maximum aperture constraints the low-frequency threshold. Here, we choose a maximum aperture of around 120–150 km (see Figure S2 in Supporting Information S1). After waveform testing, we found that it is sufficient to calculate the waveform of 300 s. For longer periods, its amplitude energy is too weak, and we will not consider it in this study. We make use of three broadband seismic arrays (CI network, see Figure S2 in Supporting Information S1 for station information) (Figure 1a) distributed on three different tectonic regions (Garlock Fault A1, Transverse Range A2, Salton Trough A3) near the plate boundary (the San Andreas fault) between the North American plate and the Pacific plate to understand its local asthenospheric anisotropy. Figure 1a shows the geometry of the stations. The red triangles in Figure 1a are defined to be the central station that outputs the translational displacement. The collection of great circle paths (Figure 1a) with enough large events provide a good azimuth coverage for the study of azimuthal anisotropy in the upper mantle.

## 4. Results

### 4.1. Rotational Motion Retrieval and Velocity Estimation

The red lines in Figure 1b show examples of derived rotational waveforms of Rayleigh waves using the A2 (Figure 1a) seismic array (see Figure S3 in Supporting Information S1 for A1 and A3 waveforms) from the earthquake M8.2 at 99 km SE of Perryville, Alaska, in 2021 (red great circle path in Figure 1a). Figure 1c shows the correlation coefficient between translation and derived rotation of the A2 array for these 110 events. The high correlation coefficient close to 1 in the period range of 120–250 s (Figure 1c) motivates us to choose this period range for our data analysis. Other period ranges are stronger affected by aperture size and noise. As illustrated in Equation 1 (see Methods section), the local phase velocity can be calculated from amplitude ratios. However, the estimated azimuth can be slightly different from the theoretical great circle path direction due to the effect of heterogeneity along the propagation path. Therefore, it is necessary to correct the azimuths before velocity

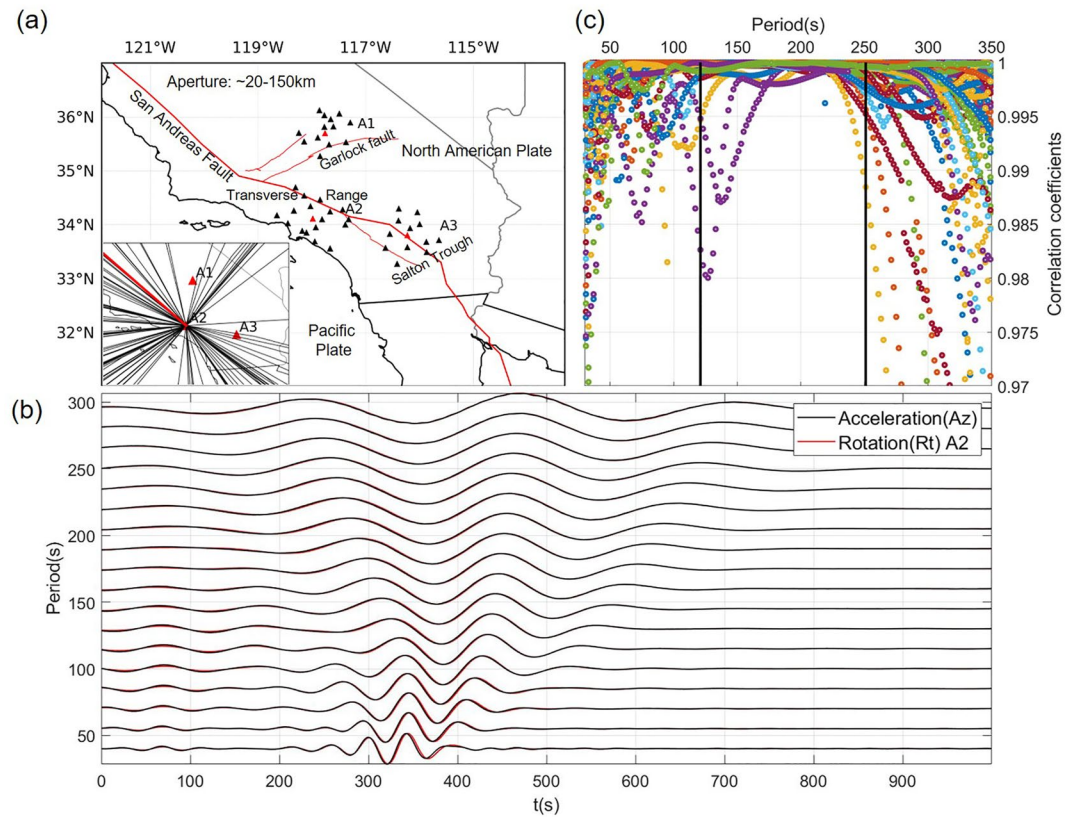


**Figure 1.** (a) Distributions of selected three seismic arrays A1, A2 and A3 and great circle paths from 110 events. The aperture of the three arrays ranges from 20 to 150 km. (b) Normalized waveform comparison between translational acceleration ( $\text{m/s}^2$ ) and retrieved rotational velocity ( $\text{rad/s}$ ) using the A2 array from the earthquake: M 8.2—99 km SE of Perryville in 2021, Alaska (the red line path in the lower left corner of a). (c) Correlation coefficients of all events between translation and retrieved rotation of the A2 array.

estimations. From a theoretical point of view, the orthogonality between rotational vector and wavenumber vector allows us to calculate the azimuth using the horizontal rotation components in a general anisotropic medium as proposed by our recent theoretical work (Tang et al., 2023). The backazimuth deviation of the A2 array compared to the theoretical great circle path direction of all events calculated using horizontal rotation (120–250 s waveform) is shown in Figure 2a, which indicates that the deviation of the angle is generally smaller than  $10^\circ$ , and most of them is within  $5^\circ$ . For the period range of 120–250 s, a  $5^\circ$  azimuth deviation is reasonable while larger deviations may be due to the error from incorrect amplitude observations and the interference with other wave types. Therefore, we only retain data with azimuth deviation within  $5^\circ$  (within the range of the red dashed line in Figure 2a). We use the weighted least-squares method (Tang et al., 2023) to estimate the phase velocity of the Rayleigh wave based on the amplitude ratio which is shown in Figures 2b–2d. The calculated average phase velocity which is marked by a black solid line is close to the theoretical value of the isotropic PREM (Preliminary Reference Earth Model) (Dziewonski & Anderson, 1981), especially for the A1 array. However, the average dispersion curve of the A2 array is slightly larger than that of PREM. In the depth range of the upper mantle corresponding to 120–250s (150–450 km), there are two uppermost mantle Transverse Ranges high-velocity anomalies beneath A2, one down to a depth of 175 km, and a second one at depths between 340 and 500 km (Schmandt & Humphreys, 2010). The relatively low velocity beneath A3, west of the Salton Trough, is attributed to partial melt in the asthenosphere as a result of lithospheric thinning (Schmandt & Humphreys, 2010).

#### 4.2. Local Azimuthal Anisotropy in the Upper Mantle

Figure 3 shows the azimuth-dependent phase velocity variation (black dots) for two periods, where the isotropic term  $c_{R0}(\omega) + \frac{1}{2c_{R0}(\omega)} R_1(\omega)$  is subtracted (see Figures S4–S6 in Supporting Information S1 for other periods).

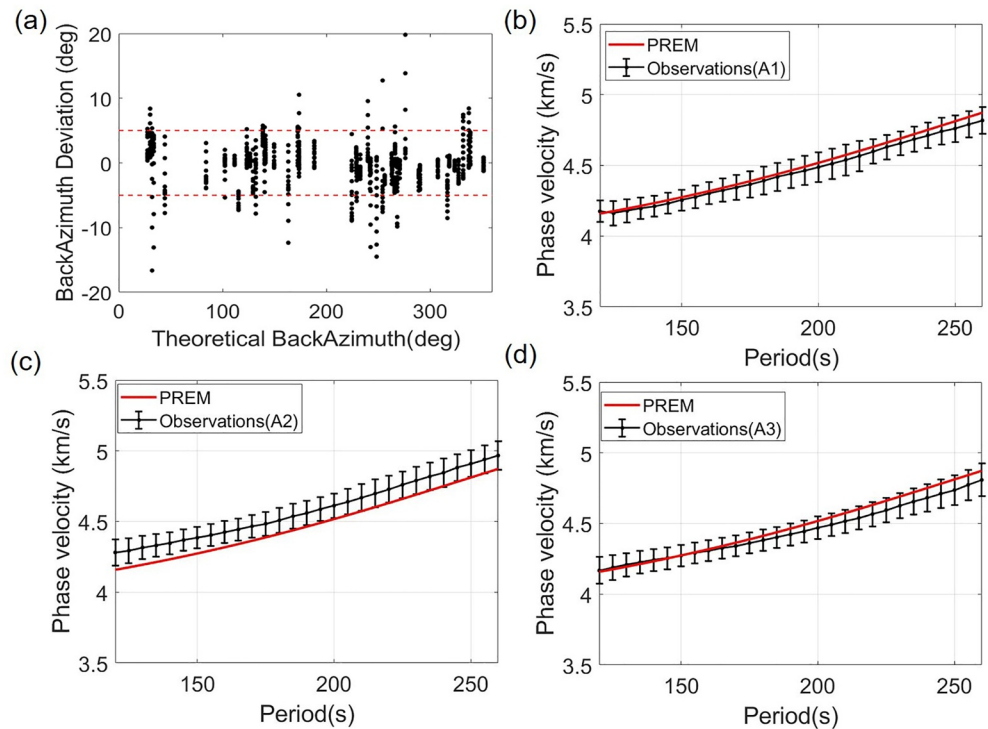


**Figure 2.** Backazimuth deviation and calculated dispersion points. Solid red line is the theoretical phase velocity from isotropic PREM model. (a) Deviations between the great circle path direction and the azimuths calculated by the horizontal rotation components (Tang et al., 2023) of the A2 array in the period range of 120–250 s (b), (c) and (d) are the observed velocity (black lines) of the three arrays calculated using only the data of the azimuth deviations (red dotted line) within 5° in (a). The  $1\sigma$  uncertainty is about 0.1 km/s.

Because the data coverage of some azimuth range is poor (see Figure 2a), and some data are not available due to large amplitude errors, we average the velocity estimates in large 120-degree azimuth bins (see Methods section). This leads to the relatively large uncertainties of phase velocity of around 0.1 km/s (Figure 3 and Figures S4–S6 in Supporting Information S1).

The red and blue curves in Figure 3 are the best-fit curves for  $2\psi$  and  $2\psi + 4\psi$  terms in Equation 1, respectively. It can be seen that the estimated phase velocity and  $2\psi$  curve fit well. The curve difference between  $2\psi$  and  $2\psi + 4\psi$  is very small (see Figure S7 in Supporting Information S1) as the  $4\psi$  term for Rayleigh waves is negligible (Montagner & Nataf, 1986). Considering the heterogeneous character of the Southern California region (Schmandt & Humphreys, 2010), the azimuthal velocity variation in the upper mantle can be the result of a mixture of heterogeneity and anisotropy. Although our method measures the local anisotropy, the influence of heterogeneity in the wavelength range cannot be ignored. To quantitatively evaluate the influence of these factors, we calculated the  $1\psi$  best-fit curve (green curve in Figure 3, Figure S7 in Supporting Information S1) and the isotropic curve misfit (black curve in Figure S7 in Supporting Information S1) to investigate the effect of a dipping formation ( $1\psi$ ) and seismic anisotropy. For most periods, the misfit of  $2\psi$  and  $2\psi + 4\psi$  is significantly smaller than the misfit of the  $1\psi$  term (Figure S7 in Supporting Information S1), indicating that the effect of anisotropy dominates. However, at the period of 130–170 s for the A1 array, 180–220 s for the A2 array, and 140–150 s for the A3 array (Figure S7 in Supporting Information S1), the misfit of  $1\psi$  is very close to that of  $2\psi$  implying that the velocity also contains the effect of local strong heterogeneity (Schmandt & Humphreys, 2010).

Even though the distance between the three arrays (about 200 km, see Figure S2 in Supporting Information S1) is much smaller than the wavelength (120–250 s: 500–1,200 km), the fast wave directions of the three arrays indicate significant differences in anisotropy pattern, especially between arrays A1 and A2 or A3. Because our approach has a local sensitivity kernel (Fichtner & Igel, 2009), mainly revealing the properties of the medium beneath the station, the lateral resolution can be several times smaller than the wavelength (see Figures S9–S12 in Supporting Information S1 for synthetic tests of lateral resolution). The peak-to-peak anisotropy strength

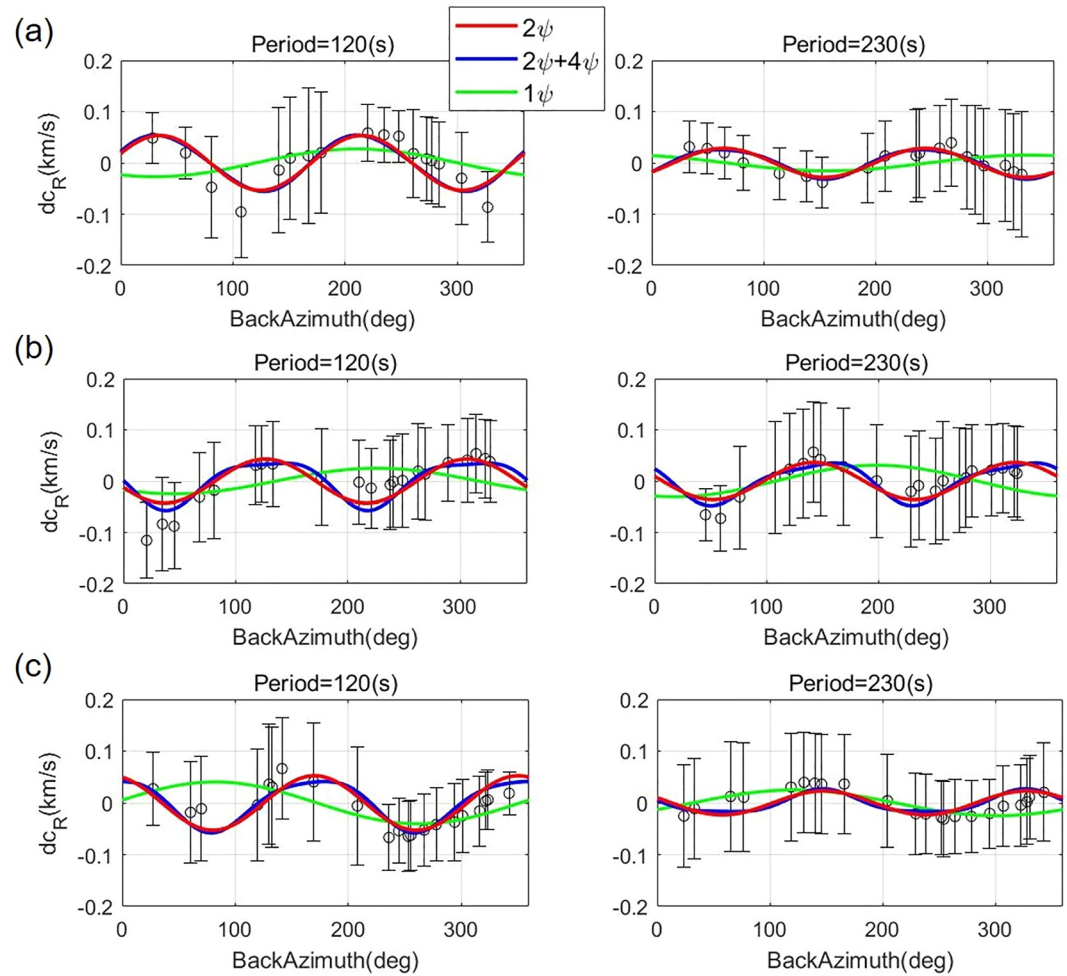


**Figure 3.** Variation of azimuth-dependent phase velocity. Red lines are the best-fit  $2\psi$  curves. Blue lines are the best-fit curves when  $2\psi$  and  $4\psi$  terms are included. Green lines are the best-fit  $1\psi$  curves. (a), (b) and (c) are the smoothed phase velocity (black points) at three different periods from the A1, A2, and A3 array, respectively. The  $1\sigma$  uncertainty (about 0.1 km/s) is estimated in an azimuth bin based on Equations 2 and 3.

fluctuates in a large range due to the error in extracting the rotation amplitude from the incomplete regular seismic array, and its strength between 0.5% and 1% (Figure S8 in Supporting Information S1) is compatible with previous studies (Alvizuri & Tanimoto, 2011; Marone & Romanowicz, 2007; Yang & Forsyth, 2006). The uncertainty in the orientation of the azimuthal anisotropy is within  $15^\circ$  for most periods, allowing us to analyze the local plate deformation of Southern California region.

## 5. Discussion

### 5.1. Mantle Flow and Plate Deformation by Local Anisotropy Observations

We estimate the corresponding depth range of anisotropic properties based on Rayleigh waves sensitivity kernels of the PREM model (Dziewonski & Anderson, 1981) and compare them with joint inversion results using SKS and surface wave data (Marone & Romanowicz, 2007), SKS results (Becker et al., 2012) and geodetic results (Barbot, 2020). At a depth of 200 km, the most sensitive periods of Rayleigh waves are in the range of 140–170 s. The fast directions (Figure 4) of the three arrays obtained by our method (blue solid lines) are in good agreement with the direction of the APM (absolute plate motion, black arrows) (Gripp & Gordon, 2002). However, the lateral resolution of tomography methods (black solid lines) is limited by the long period wavelength, making it difficult to distinguish the difference of local anisotropy between the three observation points. Even though the SKS results (green lines) display some differences in the anisotropy directions of the three arrays, the derived

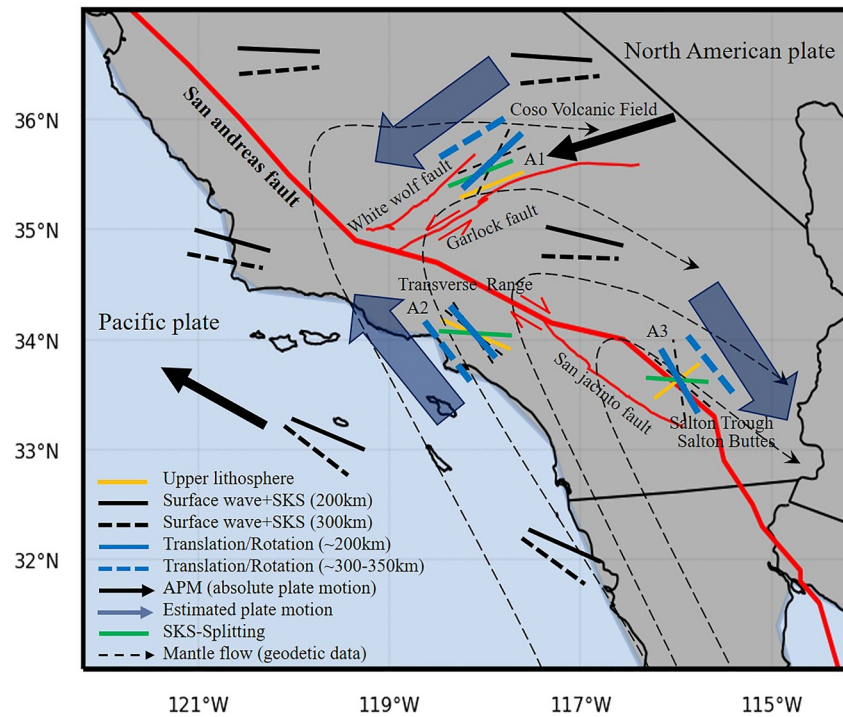


**Figure 4.** Comparison of fast wave directions from different methods. The solid black line and dashed black line represent the S-wave fast wave directions jointly retrieved by SKS and surface waves (Marone & Romanowicz, 2007) at depth of 200 and 300 km, respectively. The solid blue line and dashed blue line represent the Rayleigh wave fast directions retrieved by the amplitude ratio between translation and rotation at depth of about 200 and 300 km, respectively. The black arrow represents the APM directions (Gripp & Gordon, 2002). The green lines represent the fast directions of SKS splitting (Becker et al., 2012). The dashed black lines with arrows are the horizontal mantle flow streamlines retrieved by geodetic data (Barbot, 2020). Yellow lines represent the fast direction of Rayleigh wave in the upper lithosphere estimated from the beamforming method (Alvizuri & Tanimoto, 2011) and blue shaded arrows are estimated plate motion directions from the amplitude ratio method.

fast axis directions deviate substantially from the direction of the APM, especially at A2 and A3 arrays. Because the SKS results represent the integral effects of the whole upper mantle, making it difficult to specifically study anisotropy in the asthenosphere depth range, and to discriminate it from the strong anisotropy observed in the lithosphere of Southern California region (Alvizuri & Tanimoto, 2011; Yang & Forsyth, 2006) due to the collision of plates.

The distribution of horizontal mantle flow (black dashed lines with arrows in Figure 4) below the lithosphere obtained from geodetic data is in good agreement with the results of our amplitude-based observations, especially at A2 and A3.

The fast direction of the Rayleigh wave above the lithosphere near the A2 array (yellow lines in Figure 4) is parallel to the direction of relative motion along the San Andreas fault (Alvizuri & Tanimoto, 2011), and this anisotropy is interpreted as shear deformation from the collision of the two plates. In the asthenosphere, the fast wave direction is northwest-southeast (blue lines in Figure 4), and there is about 20° angle with respect to the fault orientation, which indicates that the anisotropy mechanism of the mantle here is different from that of the lithosphere, possibly controlled by the horizontal mantle flow (Barbot, 2020). The obvious anisotropy drop in the period range of 140–170 s (about 200 km depth, Figures S4–S6 and Figure S8 in Supporting Information S1) in three arrays provides a new evidence of layering of anisotropy probably indicating the lower boundary of the low-velocity zone (LVZ) and the significant anisotropy in the middle of LVZ (Karato, 2012). The fast direction of the asthenosphere (blue lines in Figure 4) near the A3 array is basically parallel to the plate boundary. However, its anisotropy originates from complex mantle dynamics which is not only affected by an upwelling beneath the Salton Trough (Humphreys et al., 1984; Kohler, 1999; Yang & Forsyth, 2006) (Salton Buttes, a group of volcanoes), but also a nearby return flow (Barbot, 2020), where the direction of the mantle flow is rapidly changing.



In contrast, the fast direction of the lithosphere (Alvizuri & Tanimoto, 2011) near A1 (yellow lines in Figure 4) is consistent with the results of SKS, parallel to the direction of the White Wolf and Garlock faults, while the direction of the mantle flow here (Barbot, 2020) is also parallel to the fault direction. Combining geodetic measurements and the evidence from our local anisotropy observations, the horizontal mantle flow in Southern California indeed has a sharp bend along the San Andreas fault (plate boundary), while vertical mantle flow may exist, which results in extremely complex plate deformation (wide blue shaded arrows), faulting distribution and strong heterogeneity (Tape et al., 2009), revealing its complex tectonic evolution history (Atwater, 1998). So far, we have only three points of local anisotropy measurements in Southern California. In the future, additional observations of rotation could be employed to better constrain the complex geodynamics of upper mantle regions.

## 5.2. Limitations of the ADR Approach

In our theoretical study (Tang et al., 2023), the local seismic anisotropy can be revealed by the amplitude ratio between acceleration and rotation rate. At present, there are no broadband rotational seismometers with sufficient sensitivity in the Southern California region (or elsewhere). To demonstrate the potential of our approach, we selected three high-quality seismic arrays to retrieve rotational waveforms based on the ADR approach (see Supporting Information S1) in the Southern California region. The ADR is our only choice to retrieve the rotational waveform even though it has some limitations. The period range is limited by the aperture of the seismic array, the noise level, the amplitude errors of instruments (Donner et al., 2017; Spudich & Fletcher, 2008; Spudich et al., 1995). To estimate a reliable phase velocity of Rayleigh waves, we set two key thresholds to evaluate and select available rotational waveforms. One is to quantify the similarity between translation and rotation (Figure 1). The other is to quantify the azimuth deviation between theoretical and estimated azimuths from horizontal rotation components (Figure 2).

Strong wavelength-scale heterogeneity underneath the array will undermine the assumption of homogeneity on which ADR methods are based. In addition, the non-uniformity of the geometric distribution of stations affects the phase and amplitude of the retrieved rotational waveform. Small errors in the waveform can lead to considerable deviations in the estimated velocity, which indicates that waveform quality control based on correlation coefficients (Figure 1c) is extremely important. Consequently, there is an urgent need to develop and deploy portable broadband rotational seismometers with a low noise level (Igel et al., 2021), since direct observations of rotation can eliminate the period limitation of the ADR method and errors caused by irregular deployment of stations.

A key point in the study of azimuthal anisotropy is to extract accurate backazimuths. For the surface wave with a period of 120–250 s in this paper, we assume that the deviation of its azimuth comes from waveform errors, rather than the influence of heterogeneity on the propagation path. However, strong heterogeneity, such as in the Southern California region, can lead to significant deviation in the azimuths (Alvizuri & Tanimoto, 2011), especially at the lithospheric scale. Therefore, azimuth correction is generally necessary, and Tang et al. (2023) also provides a method of estimating the backazimuth using the horizontal rotation waveform.

## 6. Conclusion

Based on the amplitude ratio between translational displacement and rotation, local structure and anisotropy can be extracted with a good lateral and vertical resolution at the same time. It allows us to recover the azimuthal anisotropy of the upper mantle and to study the plate deformation and local mantle flow with orientation changes at depth, providing new insights on geodynamic processes and tectonic evolution for the complex Southern California region. It provides strong constraints for the layering of the upper mantle anisotropy that remains poorly constrained from current seismological observations methods, SKS splitting, or surface wave tomography. While the array aperture limits the frequency range, the analysis presented should provide motivation to further improve the sensitivity of rotation sensors below the Earth's low noise level such that in the future the proposed technique could be applied to single stations. It is expected that the approach would be particularly useful whenever seismic arrays are not affordable or difficult to implement (e.g., planetary or ocean bottom observations, volcanology, urban seismology, or structural engineering).

## Data Availability Statement

All waveforms are from CI network of Southern California which are publicly available and accessed from SCEDC (2013): Southern California Earthquake Center. The SKS splitting database are available from Barruol et al. (2009). The fast direction of Rayleigh waves in the upper lithosphere are available from Alvarezuri and

Tanimoto (2011). The fast wave directions from joint inversion of surface wave data and SKS are available from Marone and Romanowicz (2007). The horizontal mantle flow directions are available from Barbot (2020). Codes and station names used in the paper are available from tangle0129 (2023).

#### Acknowledgments

This work is funded by the European Union's Horizon 2020 research and innovation program under the Marie Skłodowska-Curie grant agreement No 955515. HI gratefully acknowledges the support from the Cecil and Ida Green Foundation for visits to the Institute of Geophysics and Planetary Physics at the University of Southern California San Diego in 2022 and 2023. We are also grateful for comments from Frank Vernon and Gabi Laske. Open Access funding enabled and organized by Projekt DEAL.

#### References

- Alvizuri, C., & Tanimoto, T. (2011). Azimuthal anisotropy from array analysis of Rayleigh waves in southern California [Dataset]. *Geophysical Journal International*, *186*(3), 1135–1151. <https://doi.org/10.1111/j.1365-246X.2011.05093.x>
- Anderson, D. L., Minster, B., & Cole, D. (1974). The effect of oriented cracks on seismic velocities. *Journal of Geophysical Research*, *79*(26), 4011–4015. <https://doi.org/10.1029/jb079i026p04011>
- Atwater, T. M. (1998). Plate tectonic history of southern California with emphasis on the western transverse ranges and northern channel islands.
- Barbot, S. (2020). Mantle flow distribution beneath the California margin [Dataset]. *Nature Communications*, *11* (1), 4456. <https://doi.org/10.1038/s41467-020-18260-8>
- Barruol, G., Wuestefeld, A., & Bokelmann, G. (2009). SKS-splitting database [Dataset]. Université de Montpellier, Laboratoire Géosciences. [https://doi.org/10.18715/sks\\_splitting\\_database](https://doi.org/10.18715/sks_splitting_database)
- Becker, T. W., Lebedev, S., & Long, M. (2012). On the relationship between azimuthal anisotropy from shear wave splitting and surface wave tomography. *Journal of Geophysical Research*, *117*(B1), B01306. <https://doi.org/10.1029/2011jb008705>
- Crampin, S. (1978). Seismic-wave propagation through a cracked solid: Polarization as a possible dilatancy diagnostic. *Geophysical Journal International*, *53*(3), 467–496. <https://doi.org/10.1111/j.1365-246X.1978.tb03754.x>
- Crampin, S., Evans, R., Üçer, B., Doyle, M., Davis, J. P., Yegorkina, G. V., & Miller, A. (1980). Observations of dilatancy-induced polarization anomalies and earthquake prediction. *Nature*, *286*(5776), 874–877. <https://doi.org/10.1038/286874a0>
- Crampin, S., & Lovell, J. H. (1991). A decade of shear-wave splitting in the earth's crust: What does it mean? What use can we make of it? And what should we do next? *Geophysical Journal International*, *107*(3), 387–407. <https://doi.org/10.1111/j.1365-246X.1991.tb01401.x>
- Donner, S., Lin, C.-J., Hadziioannou, C., Gebauer, A., Vernon, F., Agnew, D. C., et al. (2017). Comparing direct observation of strain, rotation, and displacement with array estimates at piñon flat observatory, California. *Seismological Research Letters*, *88*(4), 1107–1116. <https://doi.org/10.1785/0220160216>
- Dziewonski, A. M., & Anderson, D. L. (1981). Preliminary reference earth model. *Physics of the Earth and Planetary Interiors*, *25*(4), 297–356. [https://doi.org/10.1016/0031-9201\(81\)90046-7](https://doi.org/10.1016/0031-9201(81)90046-7)
- Fichtner, A., & Igel, H. (2009). Sensitivity densities for rotational ground-motion measurements. *Bulletin of the Seismological Society of America*, *99*(2B), 1302–1314. <https://doi.org/10.1785/0120080064>
- Forsyth, D. W. (1975). The early structural evolution and anisotropy of the oceanic upper mantle. *Geophysical Journal International*, *43*(1), 103–162. <https://doi.org/10.1111/j.1365-246X.1975.tb00630.x>
- Ghosh, A., & Holt, W. E. (2012). Plate motions and stresses from global dynamic models. *Science*, *335*(6070), 838–843. <https://doi.org/10.1126/science.1214209>
- Gripp, A. E., & Gordon, R. G. (2002). Young tracks of hotspots and current plate velocities. *Geophysical Journal International*, *150*(2), 321–361. <https://doi.org/10.1046/j.1365-246X.2002.01627.x>
- Humphreys, E., Clayton, R. W., & Hager, B. H. (1984). A tomographic image of mantle structure beneath southern California. *Geophysical Research Letters*, *11*(7), 625–627. <https://doi.org/10.1029/g101i007p00625>
- Igel, H., Cochard, A., Wassermann, J., Flaws, A., Schreiber, U., Velikoseltsev, A., & Pham Dinh, N. (2007). Broad-band observations of earthquake-induced rotational ground motions. *Geophysical Journal International*, *168*(1), 182–196. <https://doi.org/10.1111/j.1365-246X.2006.03146.x>
- Igel, H., Schreiber, K. U., Gebauer, A., Bernauer, F., Egdorf, S., Simonelli, A., et al. (2021). Romy: A multi-component ring laser for geodesy and geophysics. *Geophysical Journal International*, *225*(1), 684–698. <https://doi.org/10.1093/gji/ggaa614>
- Igel, H., Schreiber, U., Flaws, A., Schuberth, B., Velikoseltsev, A., & Cochard, A. (2005). Rotational motions induced by the M8. 1 Tokachi-Oki earthquake, September 25, 2003. *Geophysical Research Letters*, *32*(8), L08309. <https://doi.org/10.1029/2004gl022336>
- Karato, S.-I. (2012). On the origin of the asthenosphere. *Earth and Planetary Science Letters*, *321*, 95–103. <https://doi.org/10.1016/j.epsl.2012.01.001>
- Kohler, M. D. (1999). Lithospheric deformation beneath the san gabriel mountains in the southern California transverse ranges. *Journal of Geophysical Research*, *104*(B7), 15025–15041. <https://doi.org/10.1029/1999jb900141>
- Marone, F., & Romanowicz, B. (2007). The depth distribution of azimuthal anisotropy in the continental upper mantle [Dataset]. *Nature*, *447*(7141), 198–201. <https://doi.org/10.1038/nature05742>
- Montagner, J.-P. (1994). Can seismology tell us anything about convection in the mantle? *Reviews of Geophysics*, *32*(2), 115–137. <https://doi.org/10.1029/94rg00099>
- Montagner, J.-P., & Nataf, H.-C. (1986). A simple method for inverting the azimuthal anisotropy of surface waves. *Journal of Geophysical Research*, *91*(B1), 511–520. <https://doi.org/10.1029/jb091ib01p00511>
- Ribe, N. M. (1989). Seismic anisotropy and mantle flow. *Journal of Geophysical Research*, *94*(B4), 4213–4223. <https://doi.org/10.1029/jb094ib04p04213>
- Savage, M. (1999). Seismic anisotropy and mantle deformation: What have we learned from shear wave splitting? *Reviews of Geophysics*, *37*(1), 65–106. <https://doi.org/10.1029/98rg02075>
- SCEDC. (2013). Southern California earthquake center [Dataset]. Caltech. <https://doi.org/10.7909/c3wd3xh1>
- Schmandt, B., & Humphreys, E. (2010). Seismic heterogeneity and small-scale convection in the southern California upper mantle. *Geochemistry, Geophysics, Geosystems*, *11*(5), Q05004. <https://doi.org/10.1029/2010gc003042>
- Schreiber, K., Gebauer, A., Igel, H., Wassermann, J., Hurst, R. B., & Wells, J.-P. R. (2014). The centennial of the SAGNAC experiment in the optical regime: From a tabletop experiment to the variation of the earth's rotation. *Comptes Rendus Physique*, *15*(10), 859–865. <https://doi.org/10.1016/j.crhy.2014.10.003>
- Schreiber, K., Velikoseltsev, A., Carr, A., & Franco-Anaya, R. (2009). The application of fiber optic gyroscopes for the measurement of rotations in structural engineering. *Bulletin of the Seismological Society of America*, *99*(2B), 1207–1214. <https://doi.org/10.1785/0120080086>
- Silver, P. G., & Chan, W. W. (1988). Implications for continental structure and evolution from seismic anisotropy. *Nature*, *335*(6185), 34–39. <https://doi.org/10.1038/335034a0>
- Smith, M. L., & Dahlen, F. (1973). The azimuthal dependence of love and Rayleigh wave propagation in a slightly anisotropic medium. *Journal of Geophysical Research*, *78*(17), 3321–3333. <https://doi.org/10.1029/jb078i017p03321>

- Spudich, P., & Fletcher, J. B. (2008). Observation and prediction of dynamic ground strains, tilts, and torsions caused by the m w 6.0 2004 Parkfield, California, earthquake and aftershocks, derived from UPSAR array observations. *Bulletin of the Seismological Society of America*, 98(4), 1898–1914. <https://doi.org/10.1785/0120070157>
- Spudich, P., Steck, L. K., Hellweg, M., Fletcher, J., & Baker, L. M. (1995). Transient stresses at Parkfield, California, produced by the m 7.4 landers earthquake of June 28, 1992: Observations from the UPSAR dense seismograph array. *Journal of Geophysical Research*, 100(B1), 675–690. <https://doi.org/10.1029/94jb02477>
- Tang, L., & Fang, X. (2023). Application of six-component ambient seismic noise data for high-resolution imaging of lateral heterogeneities. *Geophysical Journal International*, 232(3), 1756–1784. <https://doi.org/10.1093/gji/ggac406>
- Tang, L., Igel, H., & Montagner, J.-P. (2023). Single-point dispersion measurement of surface waves combining translation, rotation and strain in weakly anisotropic media: Theory. *Geophysical Journal International*, 235(1), 24–47. <https://doi.org/10.1093/gji/ggad199>
- tangle0129. (2023). spin-itn/6c\_anisotropy: Anisotropy\_rotation [Software]. Zenodo. <https://doi.org/10.5281/zenodo.8163782>
- Tanimoto, T., & Anderson, D. L. (1984). Mapping convection in the mantle. *Geophysical Research Letters*, 11(4), 287–290. <https://doi.org/10.1029/gl011i004p00287>
- Tape, C., Liu, Q., Maggi, A., & Tromp, J. (2009). Adjoint tomography of the southern California crust. *Science*, 325(5943), 988–992. <https://doi.org/10.1126/science.1175298>
- Vinnik, L., Kosarev, G., & Makeyeva, L. (1984). Anisotropy of the lithosphere from the observations of SKS and SKKS. *Proceedings of the USSR Academy of Sciences*, 278, 1335–1339.
- Yang, Y., & Forsyth, D. W. (2006). Rayleigh wave phase velocities, small-scale convection, and azimuthal anisotropy beneath southern California. *Journal of Geophysical Research*, 111(B7), B07306. <https://doi.org/10.1029/2005jb004180>
- Zhu, H., & Tromp, J. (2013). Mapping tectonic deformation in the crust and upper mantle beneath Europe and the North Atlantic Ocean. *Science*, 341(6148), 871–875. <https://doi.org/10.1126/science.1241335>